JOURNAL OF Materials CHEMISTRY

Mesoporous titanium dioxide: sonochemical synthesis and application in dye-sensitized solar cells

Yang-Qin Wang, Si-Guang Chen, Xiang-Hai Tang, Oleg Palchik, Arie Zaban,* Yuri Koltypin and Aharon Gedanken*

Department of Chemistry, Bar-Ilan University, Ramat-Gan 52900, Israel. E-mail: gedanken@mail.biu.ac.il; E-mail: zabana@mail.biu.ac.il

Received 26th July 2000, Accepted 9th November 2000
First published as an Advance Article on the web 10th January 2001

A novel method for shortening the synthesis time of mesoporous TiO_2 to 6 h is reported. Low-angle XRD and TEM showed that mesoporous TiO_2 with short-range ordered structures was synthesized when octadecylamine was used as a structure-directing agent and when $Ti(OPr^i)_4$ was used as a precursor. The highest surface area (853 $m^2\ g^{-1}$) was obtained after extraction with a dilute solution of nitric acid. The material maintained a high surface area (467 $m^2\ g^{-1}$) after calcination at 350 °C, but the short-range ordered structures collapsed. XPS showed the interaction between TiO_2 and octadecylamine, while DSC, TGA, and FT-IR spectra showed the removal of octadecylamine by extraction and calcination. A mechanism for the fast formation of mesoporous TiO_2 is proposed. It is attributed to the formation of mesoporous material at high temperatures formed in the interface between the gas and bulk solutions resulting from ultrasound irradiation. Electrodes made from the mesoporous TiO_2 were tested in a dye-sensitized solar cell. The short-circuit photocurrent, open-circuit photovoltage and fill factor increased with an increase in the sintering temperature, having a performance threshold at 450 °C, showing that the more ordered structures are required for high solar cell conversion efficiencies.

Introduction

Since the discovery of the ordered mesoporous silica M41S,[1] a variety of ordered mesoporous materials have been synthesized using the assembly of surfactant molecules as a template. These materials have a wide range of framework compositions, morphologies, and porous structures. This approach to mesostructured materials has been extended to non-silica oxides,[2–16] which might promise applications involving electron transfer, magnetic interactions, photocatalysis or catalyst support. Semiconducting transition metal oxides participate in a variety of photocatalytic reactions. Titanium dioxide is one of the most studied semiconductors for the photocatalytic reactions; it can be used in the treatment of environmental pollution, such as the photoassisted degradation of organic chloride compounds, phenol, and organic phosphorus peptides *etc.*[17] Titanium dioxide, especially in its anatase phase, has also been investigated extensively as an electrode in dye-sensitized solar cells because of its high stability toward photocorrosion, its conduction band, and its band-gap energies.[18–20] In dye-sensitized solar cells, the next two features of anatase are also important. First, TiO_2 must have an extremely high surface area, the roughness factor being 1000 for a film thickness of 10 μm. Second, it must be interconnected to allow for electronic conduction. So, generally, sintered nanometer-sized TiO_2 colloids were used as electrodes and the efficiency of the solar cells reached over 10%.[18] The mesoporous TiO_2 has a higher degree of order than the usual random fractal-like assembly of nanoparticles. Thus using it as an electrode in dye-sensitized solar cells may improve the conversion efficiency. The use of mesoporous TiO_2 would facilitate pore diffusion, give easier access to the film surface, and allow the junction to be formed under better control.[21]

Mesoporous titania has been synthesized by using alkyl phosphate surfactants,[4] octadecylamine,[6] and block copolymers,[10] as well as by employing a modified method with CTAB (cetyltrimethylammonium bromide) as a structure-directing agent.[14,16] But all of these methods require a long period of time (as long as 15 days) and the surface area after calcination is low.

Sonochemical processing has proven to be a useful technique for generating novel materials with unusual properties.[22,23] The chemical effect of ultrasound arises from acoustic cavitation, that is, the formation, growth, and implosive collapse of bubbles in a liquid. The implosive collapse of the bubbles generates localized hot spots through adiabatic compression or shock wave formation within the gas phase of the collapsing bubble. These hot spots have been shown to have transient temperatures of about 5000 K, pressures of 1800 atm, and cooling rates in excess of $10^8\ K\ s^{-1}$.[22] The application of ultrasound to the synthesis of a wide range of materials has recently been reviewed by Suslick and Price.[24]

This work is the extension of our earlier research.[25] We employed ultrasonic waves to synthesize mesoporous TiO_2 under different conditions and investigated its photoelectrochemical properties in dye-sensitized solar cells.

Experimental

Chemicals

Octadecylamine and titanium iso-propoxide [$Ti(OPr^i)_4$] were purchased from Aldrich and used without further treatment. Doubly distilled water and absolute ethanol were used as solvents. The dye Ruthenium535,$N_3$was purchased from Solaronix Co. and used and received.

Synthesis

In the synthesis of mesoporous TiO_2, $Ti(OPr^i)_4$ was dissolved in absolute ethanol. The molar ratio of octadecylamine to $Ti(OPr^i)_4$ was fixed to 1/3 and the amount of $Ti(OPr^i)_4$ was 0.01 moles. The octadecylamine was dissolved in absolute ethanol or dispersed in a mixture of ethanol and distilled water.

Table 1 The morphologies, *d*-spacing, surface areas, pore sizes, and pore volumes for the samples prepared by methods I and II

Pore volume /mL g^{-1}	Pore size/Å	Surface area/m^2 g^{-1}	*d*-Spacing/Å	Morphologies	Method
			38.5	Spherical	Method I, as-prepared
0.53	15.6	853	No	Spherical	Method I, after extraction
0.17	13.3	467	No		Method I, calcination at 350 °C
0.15	Separate	79	No	Spherical	Method I, calcination at 450 °C
			36.8	Irregular	Method II, as-prepared
0.52	21.2	612	No	Irregular	Method II, after extraction
0.26	17.8	403	No		Method II, calcination at 350 °C
0.13	Separate	35	No	Irregular	Method II, calcination at 450 °C

Method I. In this method, 0.0033 moles of an octadecylamine was dissolved in 10 mL ethanol, followed by the addition of 0.01 moles $Ti(OPr^i)_4$. The resulting solution was added slowly to 40 mL of distilled water under sonication (volume ratio of ethanol/water = 1/4). After this addition, the suspension was sonicated at ambient temperature for 6 hours using a high-intensity ultrasonic probe (Misonix, XL sonifier, 1.13 cm diameter Ti horn, 20 kHz, 100 W cm^{-2}). During sonication, the temperature of the suspension rose to 80 °C. The powder was separated by centrifugation. For removal of the surfactant, the as-prepared sample was post-treated by extraction in a dilute solution of HNO_3 in ethanol, washed three times with ethanol, and then dried overnight under vacuum. Calcination at 350 °C for 8 hours under vacuum, or at 450 °C for 4 hours under air, was also used for the removal of the octadecylamine.

Method II. In this method, the octadecylamine was dispersed in a mixture of ethanol and distilled water, and a white emulsion was formed. To this dispersion, the solution of $Ti(OPr^i)_4$ in 10 mL ethanol was added slowly under sonication (volume ratio of ethanol/water = 3/2). The initial content of chemicals and other procedures were the same as in method I.

Characterization

Low-angle (2–10°) X-ray powder diffraction (XRD) patterns were obtained using a Bruker D8 diffractometer, with Cu-Kα radiation. Transmission electron microscopy (TEM) studies were carried out on a JEOL 2000 electron microscope. The samples for TEM were prepared by dispersing the final powders in ethanol, which was dropped onto carbon–copper grids. The nitrogen adsorption and desorption isotherms at 77 K were measured using a Micromeritics instrument (Gemini 2375) after the samples had been dried at 170 °C for 1 h. BET surface areas were calculated from the linear part of the BET plot. Pore size distributions were calculated using the Barret–Joyner–Halenda (BJH) model with the Halsey equation.[26] The pore volume was measured at the $P/P_0 = 0.9947$ signal point. DSC and TGA were carried out on METTLER DSC 25 and TGA/SDTA851^e to estimate the amount of surfactant incorporated in titanium dioxide. X-Ray photoelectron spectroscopy (XPS) was used to evaluate the interactions of TiO_2 with octadecylamine. Infrared spectra were recorded employing a Nicolet (impact 410) FT-IR spectrometer and the KBr disk method.

Preparation of electrodes and measurements of the solar cells

Two kinds of mesoporous TiO_2 suspension synthesized by method I were used to prepare the solar cell electrodes. Sample (1) was a suspension of the as-prepared TiO_2. Sample (2) was TiO_2 powder which had been calcined at 450 °C for 4 hours and dispersed in a dilute solution of nitric acid (pH = 2.0).

Conductive glass substrates (Libby Owens Ford, 8 Ohm/square F-doped SnO_2) were cleaned with soap, rinsed with deionized water, and then dried in a nitrogen stream. The two TiO_2 pastes were spread on the surface of the substrates with a glass rod, using adhesive tape as spacers. After drying in air, the films prepared with sample (1) were sintered overnight (over 12 hours) at 250 °C, 350 °C, and 450 °C. The electrodes made from sample (2) were sintered at 450 °C for 0.5 hours. All of the electrodes were sintered in air. The thicknesses of the TiO_2 films obtained above, as measured with a profilometer (Mitutoyo, Surftest SV 500), were about 1 μm. The dye [*cis*-bis(isothiocyanato)bis(2,2′-bipyridyl-4,4′-dicarboxylato)ruthenium(II)] azide was used to sensitize the electrodes by immersing the electrodes in a 5.0×10^{-4} mol L^{-1} solution of dye in absolute ethanol overnight. To remove water, the films were heated to 150 °C and cooled down to 80 °C prior to immersion in the dye solution.

A sandwich-type configuration was employed to measure the performance of the dye-sensitized solar cells, using the Pt-coated F-doped SnO_2 film as a counter electrode. Illumination of the cell was effected with a calibrated Xe lamp and direct sunlight. An Eco Chemie potentiostat was used to measure the photocurrent and photovoltage.

Results and discussion

Synthesis of mesoporous TiO_2

Mesostructured TiO_2 was obtained by ultrasound irradiation, using octadecylamine as a structure-directing agent and $Ti(OPr^i)_4$ as a precursor. Two series of samples with different morphologies and different surface areas were obtained when octadecylamine was dissolved in ethanol or dispersed in the mixture of ethanol and distilled water. In Table 1, we have summarized the results of the morphologies, *d*-spacing values, surface areas, pore sizes, and pore volumes obtained for the as-prepared and post-treated samples. The detail will be discussed later.

Spherical or globular particles with particle sizes of 50–200 nm were obtained for the as-prepared sample synthesized by method I. Fig. 1A illustrates the TEM image of the as-prepared sample. It clearly shows that the spherical or globular particles are aggregates of very small particles and displays the short-range ordered structures. Figs. 1B and 1C present the TEM images of the samples after extraction and calcination at 450 °C, respectively. The inset in Fig. 1C is an electron diffraction pattern for the sample calcined at 450 °C, which shows the formation of the anatase phase. This concurs with the results of wide-angle XRD for the heated sample.[25]

The low- and wide-angle XRD patterns, as well as the adsorption–desorption isotherms of the samples synthesized using method I have been discussed elsewhere.[25]

A white emulsion was obtained when octadecylamine was dispersed in a mixture of ethanol and distilled water (method II). Inter-grown fundamental particles having a rough, uneven surface were obtained. The TEM image of the as-prepared sample is shown in Fig. 2A. The inter-growth of small primary particles results in aggregation and short-range ordered structures. Figs. 2B and 2C show the TEM pictures of the sample after extraction and calcination at 450 °C for 4 h, respectively. The irregular particles are the aggregations of small particles. A broad peak (36.8 Å) in the low-angle XRD was detected for this system as well (Fig. 3), indicating the short-range ordered framework structures.

A high surface area was also measured for the products synthesized using method II. After acid extraction, the surface

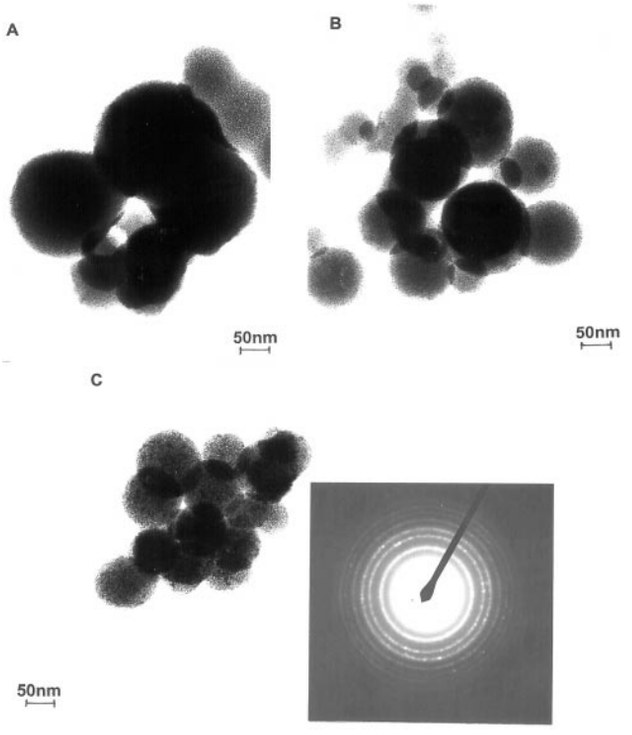

Fig. 1 TEM images of the samples synthesized using method I. (A) As-prepared sample; (B) after extraction; (C) after calcination at 450 °C for 4 h. The inset in C is the electron diffraction pattern for heated samples.

area was 612 $m^2 g^{-1}$, with a pore size of 2.1 nm and pore volume of 0.52 mL g^{-1}. After calcination at 350 °C for 8 h, a surface area of 403 $m^2 g^{-1}$ was measured. However, calcination at 450 °C for 4 h reduced the surface area to 35 $m^2 g^{-1}$. The reduction of the surface areas upon calcination is similar to that obtained for the products synthesized by method I. Fig. 4 shows the adsorption–desorption isotherms of the post-treated samples. The removal of the surfactant is by extraction or by calcination. The inset in Fig. 4 depicts the pore size distribution. The pore size distribution is broad and peaks at 21.2 Å after extraction; after calcination at 350 °C, the pore size distribution becomes narrower and peaks at 17.8 Å. The pore sizes after extraction or calcination of mesostructures synthesized by method II are larger than for those prepared by method I.

We have given an explanation for the formation of mesoporous TiO_2 based on the "neutral templating synthesis mechanism" proposed by Tanev and Pinnavaia.[27] When octadecylamine and $Ti(OPr^i)_4$ were dissolved in ethanol, the H-bonding between octadecylamine and the titanium precursor initiates the formation of rod-like micelles. Further hydrolysis and condensation of the titanium precursor produces short-range hexagonal packing. When octadecylamine was dispersed in the mixture of ethanol and distilled water, an emulsion was formed. The primary particles form and inter-grow at the surface of colloid particles of the free surfactant in emulsion form. As the primary particles undergo further inter-growth and deplete the emulsion, irregular particles with high textural mesoporosity form.

Formerly, hydrothermal treatment[28,29] was used to accelerate the condensation of the hydrolyzed products and enhance the thermal and hydrothermal stability, but it requires a long period of time. Ultrasound irradiation produces localized hot spots through adiabatic compression or shock wave formation within the gas phase of the collapsing bubble. The high temperature at the interface of the collapsing bubble and the bulk solution can accelerate the condensation of titanium hydroxyl and shorten the synthesis time. Fast condensation can enhance the thermal stability.[30]

DSC and TGA

Fig. 5a displays the DSC pattern of the as-prepared sample from method I, indicating that there is a shallow endothermic peak in the range of 0–200 °C, corresponding to desorption of water and ethanol adsorbed on the surface of mesoporous TiO_2. From 200 to 550 °C, there is a broad exothermic peak, which is resolved into two peaks at about 370 °C. We suggest that they should belong to one broad peak, corresponding to the crystallization of amorphous TiO_2. The valley between the peaks is due to an endothermic process for the removal of octadecylamine. The TGA weight loss in Fig. 5b indicates the removal of octadecylamine in the range 130–460 °C, corresponding to a weight loss of *ca.* 27%. Another weight loss level in TGA is in the range of 0–130 °C, which corresponds to the removal of adsorbed water and ethanol (*ca.* 6%). At high temperatures, there is a slow weight loss, attributed to the loss of water that is produced by the condensation of neighboring terminal hydroxyl groups. The rise of the exothermic peak is observed at 200 °C, which seems to contradict the determination of the crystallization temperature as 450 °C. The exothermic curve rises at 200 °C as a result of an inter-particle sintering effect that has already started at this temperature.

XPS

The as-prepared sample from method I was also characterized by X-ray photoelectron spectroscopy (XPS). The XPS spectrum shows the presence of oxygen, titanium, carbon, and nitrogen. The primary parameter studied was the

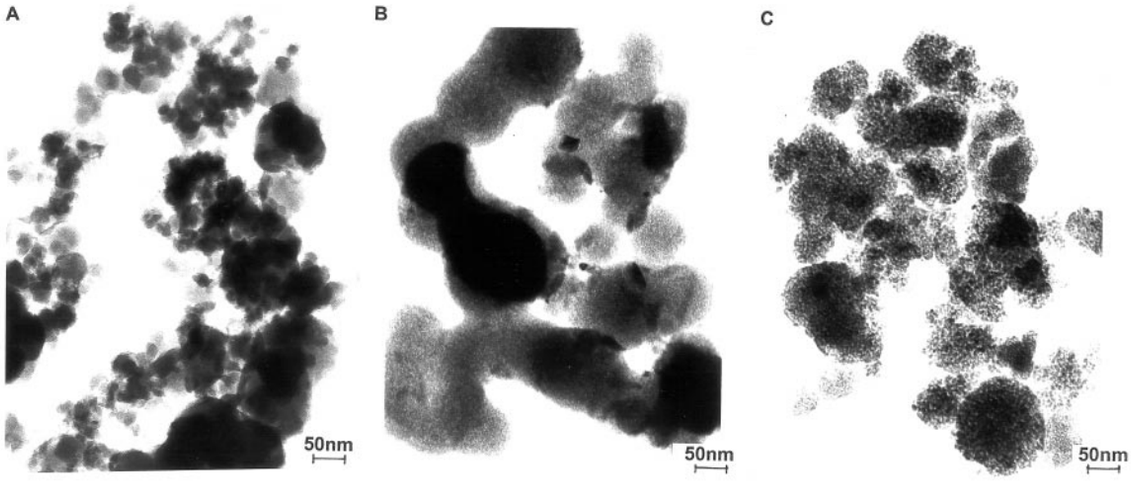

Fig. 2 TEM images of the as-prepared sample (method II) (A); after extraction (B); after calcination at 450 °C (C).

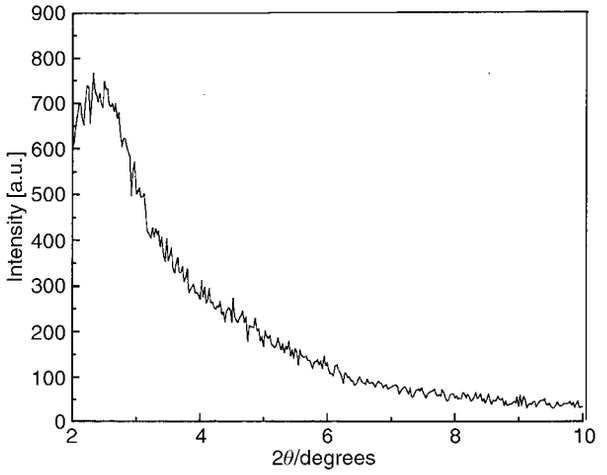

Fig. 3 Low-angle XRD pattern for the as-prepared sample from method II.

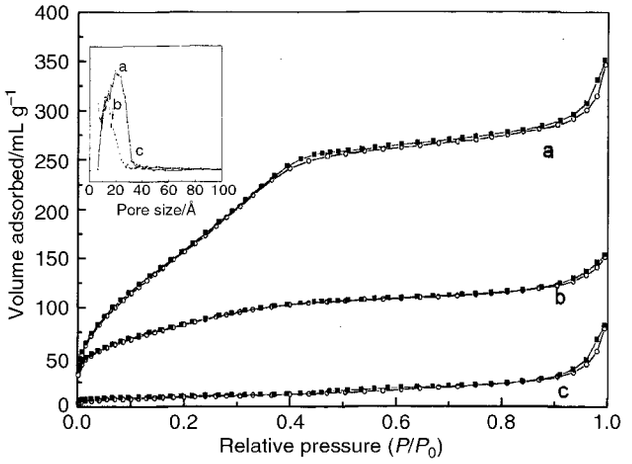

Fig. 4 Adsorption (○)–desorption (■) isotherms for the samples synthesized using method II. (a) After extraction; (b) after calcination at 350 °C; (c) after calcination at 450 °C. The inset is the pore size distribution.

coordination of titanium by measuring the binding energy of the Ti_{2p} core electron, which is 457.1 eV (Fig. 6). Fig. 7 depicts the XPS spectrum for mesoporous TiO_2 calcined at 450 °C, the nitrogen peak has disappeared and the binding energy of $Ti_{2p3/2}$ is located at 459.2 eV, corresponding to the value for anatase/rutile.[31] The red shift in the $Ti_{2p3/2}$ peak position from anatase to the mesoporous structure indicates a change of micro-enviroments for titanium. This shift is due to the interaction of octadecylamine with TiO_2.

FT-IR study

The FT-IR spectra were used to detect whether or not octadecylamine was removed by extraction or calcination. Fig. 8 shows the FT-IR spectra for the samples before and after post-treatment. Fig. 8a shows the FTIR spectrum of the as-prepared sample. The broad bands between 3000 and 3500 cm^{-1} are due to N–H stretches of octadecylamine and O–H stretches of adsorbed water. The two sharp bands at 2800–2900 cm^{-1} are due to C–H stretches of the hydrocarbon chain of octadecylamine. The weak bands at 1385 cm^{-1} and 1475 cm^{-1} are attributed to the C–H stretches of the CH_3– and –CH_2– groups in octadecylamine. These bands provide evidence for the incorporation of octadecylamine into the hydrous oxide. Figs. 8b and 8c show that the bands due to octadecylamine disappear after extraction or calcination. The broad peak at 3500 cm^{-1} and the sharp peak at 1385 cm^{-1} in

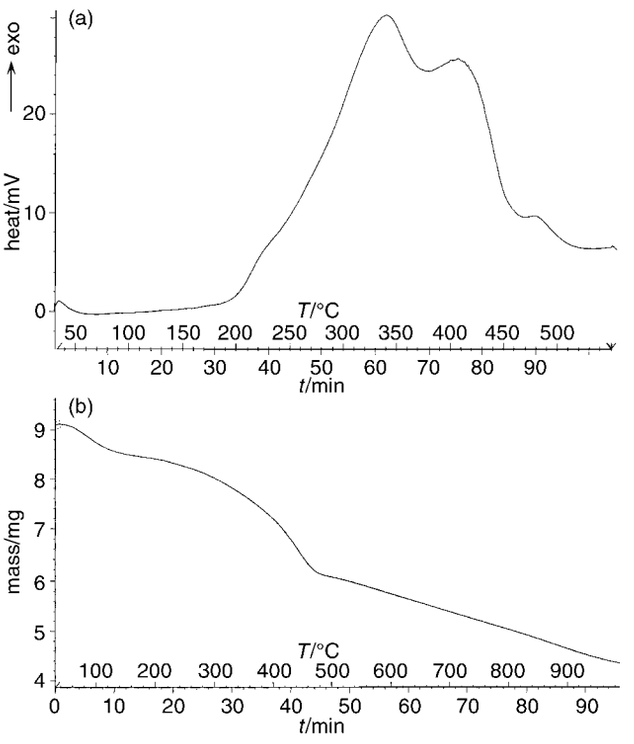

Fig. 5 DSC (a) and TGA (b) profiles for the as-prepared sample.

Fig. 8b are attributed to vibrational bands of ethanol adsorbed on the surface of TiO_2. The peak at 1620 cm^{-1} in Figs. 8a and 8b is attributed to CO_2 adsorbed onto the surface of TiO_2 which is reduced by the calcination process.

Application in dye-sensitized solar cells

In 1991, O'Regan and Grätzel first reported a 10% conversion efficiency for the dye-sensitized solar cells.[21] The high conversion efficiency is attributed to the high surface area of TiO_2 electrodes. These electrodes made from anatase TiO_2 colloids, with a surface area of 80–120 $m^2\ g^{-1}$, provided the needed surface for a dye monolayer to yield a significant optical density. The above-reported high surface area of 850 $m^2\ g^{-1}$ obtained with mesoporous TiO_2 makes this material attractive for dye-sensitized solar cells. Using such a huge surface area, it is expected that a given optical density can be achieved with thinner electrodes than those which are commonly used. By doing so, the mean path of injected electrons should be shortened, which is expected to increase the collection efficiency of the cells, thus improving their overall effectiveness.

Table 2 summarizes the results of the cell parameters for the solar cells fabricated from the two kinds of TiO_2 electrodes, as a function of the sintering temperature. Fig. 9 depicts the I–V curve for the solar cell fabricated from sample (1), which was sintered at 450 °C overnight.

It can be seen from Table 2 that the sintering temperature has a significant influence on the performance of these electrodes in dye-sensitized solar cells. Increasing the sintering temperature results in an increase in all of the cell parameters, including the photovoltage (V_{oc}), photocurrent (J_{sc}), and fill factor and thus in the maximum power achieved by the solar cell. Going from 250 °C to 450 °C, the photocurrent increases by an order of magnitude for each 100 °C step. The corresponding photovoltage almost doubles itself, while the fill factor increases by 10%. The results presented in Table 2 indicate that a major change occurs when the electrodes are sintered at 450 °C.

Gregg and coworkers[32] utilized anatase TiO_2 colloids to fabricate electrodes, which were sintered at 150 °C overnight.

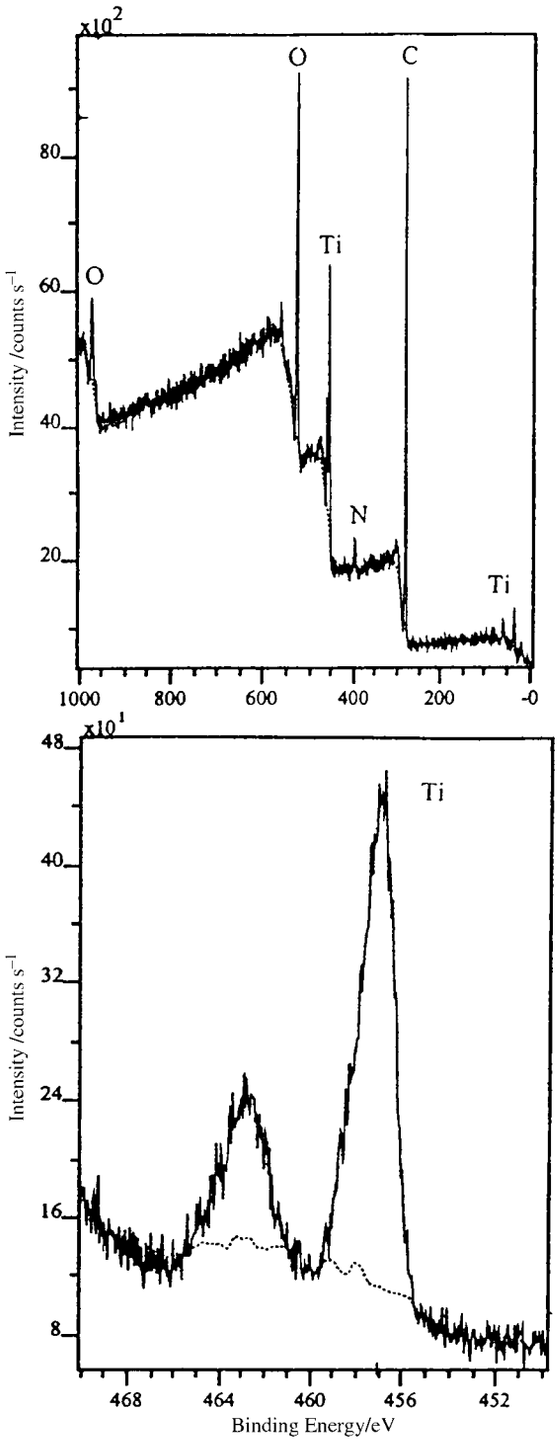

Fig. 6 XPS spectra for the as-prepared sample synthesized by method I.

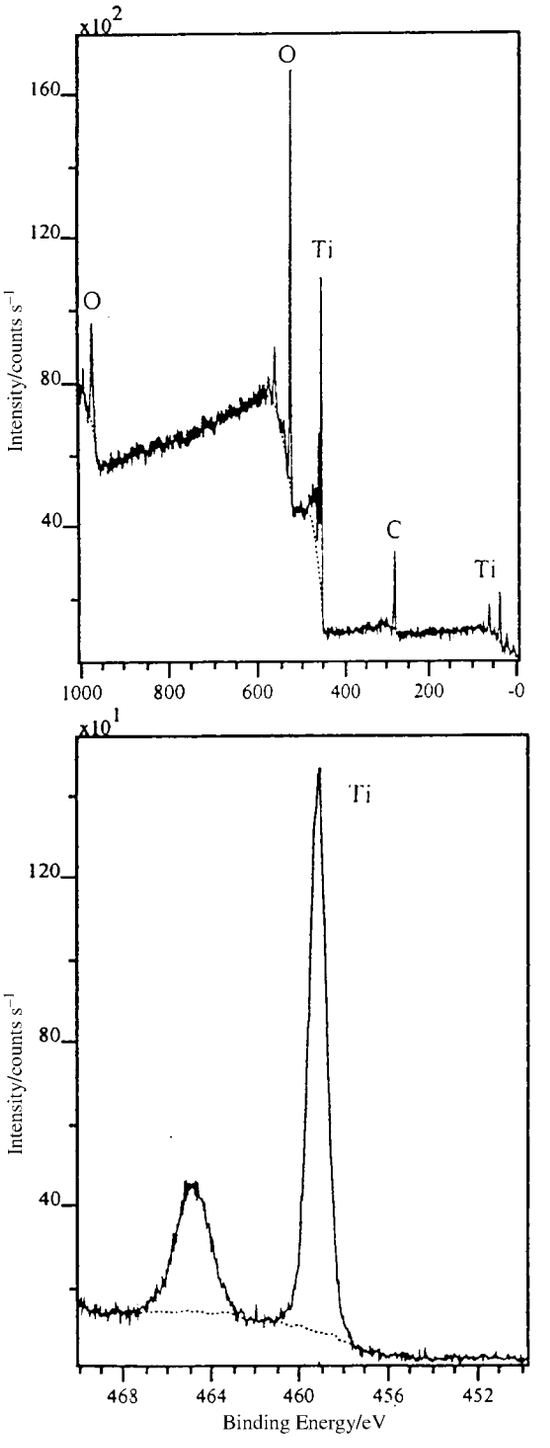

Fig. 7 XPS spectra for the sample calcined at 450 °C, method I.

These electrodes performed well in dye-sensitized solar cells, despite the low sintering temperature. This indicates that the huge increase in the cells performance upon increase of the sintering temperature is not related to the quality of the electrical contact between the colloids. Another possibility relates to the crystallinity of the TiO_2. As mentioned above, the mesoporous TiO_2 prepared by this method is amorphous. Sintering at 450 °C converts the amorphous mesoporous TiO_2 to polycrystalline anatase. The crystallization of the TiO_2 is therefore believed to be the main reason for the huge change in performance induced by the sintering process. For this reason,

Table 2 Comparison of dye-sensitized solar cells fabricated from samples (1) and (2)

Sample	Sintering temperature/°C	Sintering time/h	Efficiency (%)	V_{oc}/mV	J_{sc}/mA cm^{-2}	FF (%)
(1)	250	Over 12	0.0001	181	0.002	31.6
(1)	350	Over 12	0.0073	362	0.040	50.5
(1)	450	Over 12	1.5	669	3.502	62.2
(2)	450	0.5	1.04	694	2.403	62.2

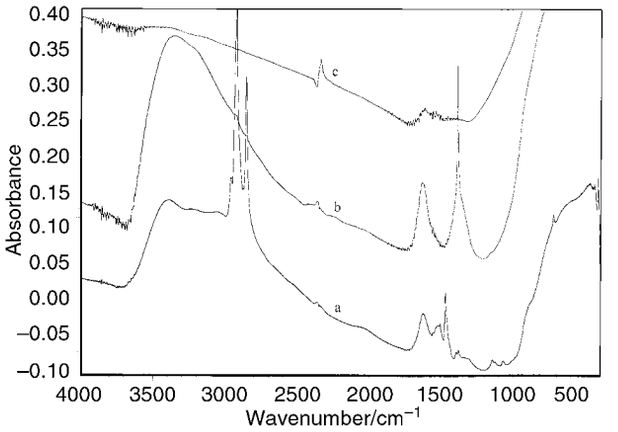

Fig. 8 FT-IR spectra for the sample: (a) as-prepared; (b) after extraction; (c) after calcination at 350 °C for 8 h.

high photovoltaic values were obtained for samples (1) and (2), but only when sample (1) was sintered at 450 °C overnight.

The solar cell measurements reported above indicate that this mesoporous TiO_2 is not thermally stable. When it is sintered, the mesopores are blocked and the surface area decreases rapidly. In this form, the resulting material is inferior to standard crystalline TiO_2. Further research, aimed at improving the thermal stability of the mesoporous TiO_2, is currently being performed in order to maintain the mesoporous properties and high surface area after phase transformation.

Conclusions

Mesoporous titanium dioxide with short-range ordered framework structures was synthesized under ultrasound irradiation, using long-chain octadecylamine as the structure-directing agent and titanium iso-propoxide as the precursor. The morphologies of the particles and associated adsorption–desorption isotherms were correlated with whether or not octadecylamine was dissolved in ethanol or dispersed in a mixture of water and ethanol. When octadecylamine was dissolved in ethanol, spherical or globular particles were obtained as aggregates of small primary particles. There was a broad peak in the low-angle XRD pattern and the as-prepared sample had a high surface area after extraction or calcination at 350 °C. When octadecylamine was dispersed in a mixture of water and ethanol, irregular inter-grown aggregates of small particles were obtained, and the hysteresis loops in the adsorption–desorption isotherms appeared at a high relative pressure, indicating the formation of textural structures.

The mesoporous TiO_2 can be utilized to fabricate the electrodes for dye-sensitized solar cells. The different sintering temperature has a great influence on the performance of the solar cells because of the phase transformation from amorphous to anatase. The maximum photovoltage, photocurrent and fill factor for mesoporous TiO_2-modified solar cells can reach 0.698 V, 3.5 mA cm^{-2} and 62%, respectively. The reason for these low parameters is attributed to the small amount of dye adsorbed. This indicates that this mesoporous TiO_2 is not thermally stable.

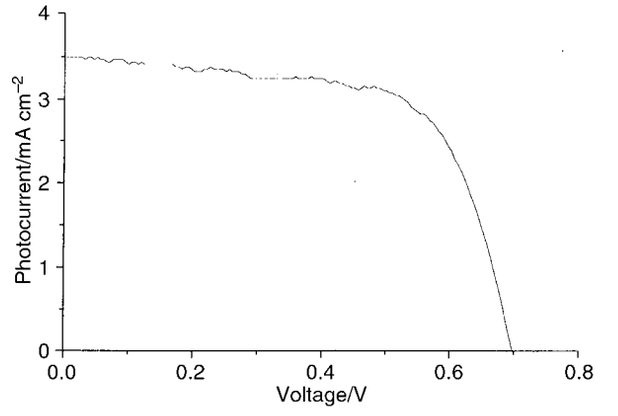

Fig. 9 *I–V* curve for the dye-sensitized solar cell fabricated from sample (1), sintered at 450 °C overnight.

Acknowledgements

Y. Q. Wang, S. G. Chen, and X. H. Tang thank the Kort 100 Scholarship Foundation for supporting their postdoctoral fellowships. This work was supported in part by the Israel Science Foundation, founded by the Israel Academy of Science and Humanity. We all thank Dr Y. Gofer for the XPS measurements and Dr S. Avivi for the measurements of DSC and TGA. The assistance of Dr Shifra Hochberg with the English editing of the paper is gratefully acknowledged.

References

1 C. T. Kresge, M. E. Leonowicz, W. J. Roth, J. C. Vartuli and J. S. Beck, *Nature*, 1992, **359**, 710.
2 D. M. Antonelli and Y. J. Ying, *Chem. Mater.*, 1996, **8**, 874.
3 Z. R. Tian, W. Tong, J. Y. Wang, N. G. Duan, V. V. Krishnan and S. L. Suib, *Science*, 1997, **276**, 926.
4 D. M. Antonelli and Y. J. Ying, *Angew. Chem., Int. Ed. Engl.*, 1995, **34**, 2014.
5 D. M. Antonelli and Y. J. Ying, *Inorg. Chem.*, 1996, **35**, 3126.
6 D. M. Antonelli, *Microporous Mesoporous Mater.*, 1999, **30**, 315.
7 U. Ciesla, S. Schacht and G. D. Stucky, *Angew. Chem., Int. Ed. Engl.*, 1996, **35**, 541.
8 P. Liu, T. Liu and A. Sayari, *Chem. Commun.*, 1997, 557.
9 G. S. Attard, *Science*, 1997, **278**, 838.
10 N. Ulagappan and C. N. R. Rao, *Chem. Commun.*, 1996, 1685.
11 P. D. Yang, D. Y. Zhao, D. L. Margolese, B. F. Chmelka and G. D. Stucky, *Nature*, 1998, **396**, 152.
12 P. V. Braun, P. Osenar, V. Tohvev, S. B. Kennedy and S. I. Stupp, *J. Am. Chem. Soc.*, 1999, **121**, 7302.
13 M. L. MacLachlan, N. Coombs, R. L. Bedard, S. White, L. K. Thompson and G. A. Ozin, *J. Am. Chem. Soc.*, 1999, **121**, 12005.
14 D. Khushalani, G. A. Ozin and A. Kuperman, *J. Mater. Chem.*, 1999, **9**, 1491.
15 L. M. Qi, J. M. Ma, H. M. Cheng and Z. Zhao, *Langmuir*, 1998, **14**, 2579.
16 D. T. On, *Langmuir*, 1999, **15**, 8561.
17 M. R. Hoffmann, S. T. Martin, W. Choi and D. W. Bahnemann, *Chem. Rev.*, 1995, **95**, 69.
18 B. O'Regan and B. M. Grätzel, *Nature*, 1991, **352**, 737.
19 M. K. Nazeeruddin, A. Kay, L. Rodicio, R. Humphry-Baker, E. Müler, P. Liska, N. Vlachopoulos and M. Grätzel, *J. Am. Chem. Soc.*, 1993, **115**, 6382.
20 A. Hagfeldt and M. Grätzel, *Chem. Rev.*, 1995, **95**, 45.
21 M. Grätzel, *Curr. Opin. Colloid Interface Sci.*, 1999, **4**, 314.
22 K. S. Suslik, *Ultrasound: Its Chemical, Physical and Biological Effects*, VCH, Weinheim, 1998.
23 K. S. Suslick, S. B. Choe, A. A. Cichowlas and M. W. Grinstaff, *Nature*, 1991, **353**, 414.
24 K. S. Suslick and G. J. Price, *Ann. Rev. Mater. Sci.*, 1999, **29**, 295.
25 Y. Q. Wang, X. H. Tang and A. Gedanken, *Adv. Mater.*, 2000, **12**, 1183.
26 S. J. Gregg and K. S. Sing, *Adsorption, Surface Area and Porosity*, Academic Press, London, 1982.
27 P. T. Tanev and T. J. Pinnavaia, *Science*, 1995, **267**, 865.
28 Q. Huo, D. I. Margolese and G. D. Stucky, *Chem. Mater.*, 1996, **8**, 1147.
29 G. D. Stucky, Q. Huo, A. Firouzi and B. F. Chmelka, *Directed Synthesis of Organic/Inorganic Composite Structures, Studies in Surface Science and Catalysis*, vol. 105, Elsevier Science B.V., Amsterdam, 1997, p. 69–76.
30 A. Corma, *Chem. Rev.*, 1997, **9**, 2373.
31 M. Murato, K. Wakino and S. Ikeda, *J. Electron Spectrosc. Relat. Phenom.*, 1975, **6**, 459.
32 F. Pichot, S. Ferrere, R. J. Pitts and B. A. Gregg, *J. Electrochem. Soc.*, 1999, **146**, 4324.